

# Experimental Investigation of FRP contribution in reinforced concrete T-beams strengthened in shear with different strengthening schemes

Jonathas F. O. Iohanathan<sup>a\*</sup>, Guilherme S. S. A. Melo<sup>b</sup>

<sup>a</sup>Federal Institute of Ceará, Morada Nova, Ceará, Brazil, jonathas.oliveira@ifce.edu.br

<sup>b</sup>University of Brasília, Brasília, Distrito Federal, Brazil. melog@unb.br

\* Corresponding author

<https://doi.org/10.1590/1679-78258141>

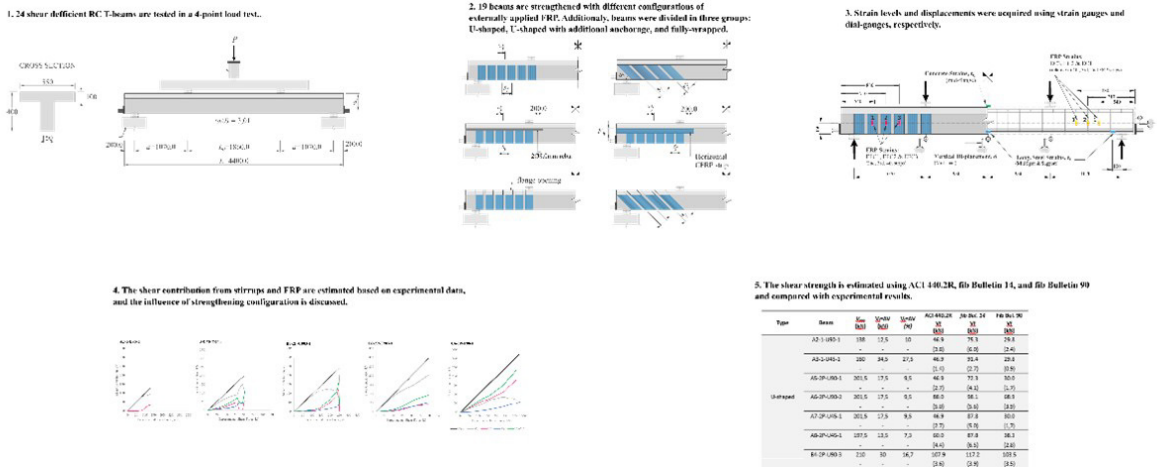
### Abstract

This study presents an experimental investigation on the contribution of carbon fiber-reinforced polymer (CFRP) sheets in shear-strengthened beams with different strengthening schemes. Three different reinforcement types and strengthening schemes are applied (U-shaped, U-shaped with additional anchorage and fully-wrapped). The strength contribution of FRP sheets, internal stirrups, and concrete are estimated based on experimental data. Two different anchoring strategies to prevent the FRP strengthening from debonding were also present, using horizontal strips of FRP and rebars on grooves on the web of the beams. The behavior of each of the beams is discussed in terms of load-displacement, failure mode, strains distribution, cracking pattern, and shear force contribution. The influence of the strengthening configuration and FRP anchorage on the FRP shear contribution and total shear resistance is discussed based on the experimental. The individual contribution of FRP, stirrups and concrete are estimated based on strain data from the tests. Finally, the experimental shear capacity is compared to the recommendations of ACI 440.2R, and fib Bulletins 14 and 90.

### Keywords

Shear strengthening, fiber reinforced polymers, shear strength, interaction, testing, repair, composites.

### Graphical Abstract



Received: abr. 3, 2024. In revised form: jun. 21, 2024. Accepted: ago. 05, 2024. Available online: ago. 13, 2024.

<https://doi.org/10.1590/1679-78258141>

Latin American Journal of Solids and Structures. ISSN 1679-7825. Copyright © 2024. This is an Open Access article distributed under the terms of the [Creative Commons Attribution License](https://creativecommons.org/licenses/by/4.0/), which permits unrestricted use, distribution, and reproduction in any medium, provided the original work is properly cited.

## 1 INTRODUCTION

Fiber-reinforced polymers (FRP) are composite materials that have been used in strengthening reinforced concrete members as an alternative to traditional materials, i.e., concrete and steel. Their high strength-to-self-weight and high stiffness, low corrosion susceptibility, and versatility are some of the aspects that make them an attractive material in strengthening reinforced concrete structures.

Strengthening reinforced concrete beams with FRP sheets against shear is a common topic in the experimental investigations present in existing literature. Several experimental programs investigate the effects of FRP strengthening on the ultimate shear capacity, the comparison between different strengthening schemes, different anchorage types and the influence of the longitudinal reinforcement ratios on the shear strength of strengthened beams (Bousselham and Chaallal, 2006; Khalifa and Nanni, 2000; Chen et al., 2016; Chen et al., 2017; Karzad et al., 2019; Siddika et al., 2019; Fu et al., 2018; Al-Saidy et al., 2010; Li and Leung, 2017; Yu et al., 2019; Araújo, 2002; Salles Neto, 2000; Silva Filho, 2001).

However, predicting the shear resistance in FRP-strengthened members is still an open research topic. There is still no consensus on the quantification of the individual contribution of each material (steel, concrete, and FRP) to the ultimate strength of the reinforced member. Among the reasons is the complexity of the shear phenomenon in reinforced concrete members itself, the interaction between the internal reinforcements and the FRP reinforcement, and the early detachment of the FRP in the case of elements externally reinforced with U-shaped FRP.

The theoretical models for predicting the shear strength of reinforced concrete elements strengthened with FRP adopted in some codes and recommendations (ACI Committee 440, 2017; Fib, 2001, 2019; National Research Council Advisory Committee on Technical Recommendations for Construction, 2004; German Committee for Reinforced Concrete, 2013) estimate the ultimate shear strength as a sum of individual and independent contributions of concrete, steel, and external FRP. Such models consider that the steel of stirrups yields at the ultimate load. However, the presence of FRP can limit the shear-critical crack opening and, consequently, limiting the strains and stresses in the internal shear reinforcement, which may not yield (Colotti, 2013). This phenomenon is the interaction between inner steel reinforcement and FRP externally bonded reinforcement. Many authors have reported the existence and the importance of considering the interaction of steel and FRP sheets (Colotti, 2013; Pellegrino and Modena, 2002; Deniaud and Cheng, 2003; Monti and Liotta, 2007; Spinella, 2019; Oller, Pujol and Marí, 2019).

The non-consideration of this interaction may lead to an under mobilization of internal steel reinforcement before FRP reaches its ultimate strain. The consideration of the interaction can contribute to a better characterization of the failure mode and thus improve the precision of the prediction of the maximum resistant capacity of the reinforced members and the contribution of each material individually. Furthermore, the codes usually consider that the FRP contribution to strength can be estimated as the difference in strength between similar beams with and without the FRP strengthening. This is an indirect way of estimating the FRP contribution, and may not account for a possible interaction between the different sources of resistance (concrete, stirrups and FRP). An alternative way of estimating the contribution of each of the contributing parts is by means of experimental data, i.e. by experimentally measuring strains, and using appropriate constitutive models for the materials one can predict their individual shear contribution.

This paper presents the results of an experimental program on externally bonded carbon-FRP ('FRP' is adopted throughout this text, as only carbon fiber is used in FRP systems) shear strengthened reinforced concrete T-beams with different strengthening configurations. The influence of the different strengthening schemes on the ultimate shear strength, failure mode, and the contribution of each individual material are presented and discussed based on the experimental results. Researches which try to estimate the FRP contribution directly based on measured strains are scarce. Even though previous papers present and estimative of the contribution based on measured strains (Oller, Pujol and Marí, 2019; Autrup, Jørgensen and Hoang, 2023). The present research evaluates the influence of the strengthening scheme on the individual contribution to the shear capacity of the concrete, internal shear reinforcement, and external FRP shear strengthening, and studies like this are not present in the literature, according to the authors' knowledge.

## 2 EXPERIMENTAL PROGRAM

The experimental program comprises 24 large-scale reinforced concrete beams tested in three series, A, B, and C, each one with 8 beams. Different internal reinforcement, strengthening layouts and anchorage systems were used in each set, as will be described in the following.

### 2.1 Geometry of beams

The experimental program consists of 24 T-shaped reinforced concrete beams. The beams are 4400 mm long, with 4000 mm between supports, and a shear span of 1070 mm. The T-section has a flange of 550 mm width, and 100 mm

thick. The total depth of the section is 400 mm, and the web thickness 150 mm. The beams are tested in a four-point bending configuration (Stuttgart Test). Figure 1 presents the geometry of the specimens and the test setup.

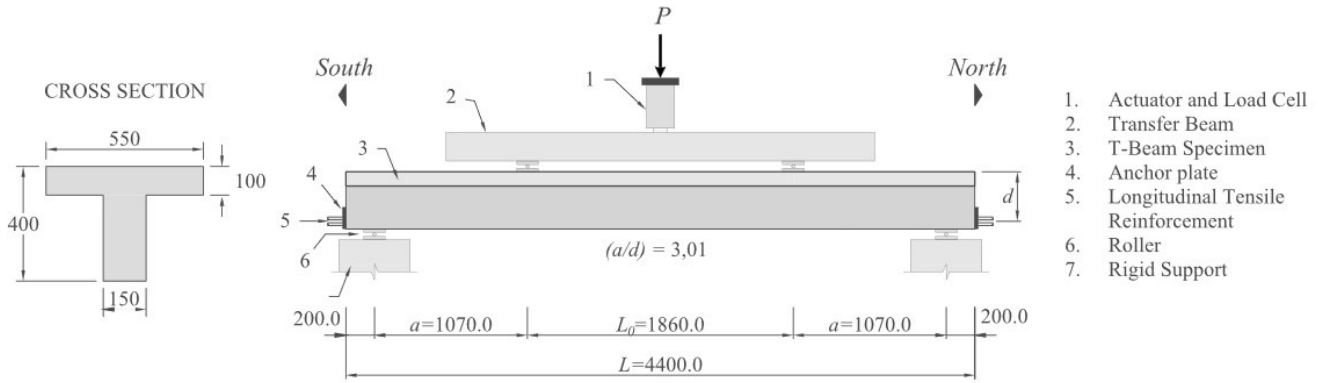


Figure 1 Test setup and dimensions of beams (in mm).

### 2.2 Internal steel reinforcement

Three different sets of internal steel reinforcement were used, namely Type 1, 2, and 3. Details of the reinforcement types are shown in Figure 2.

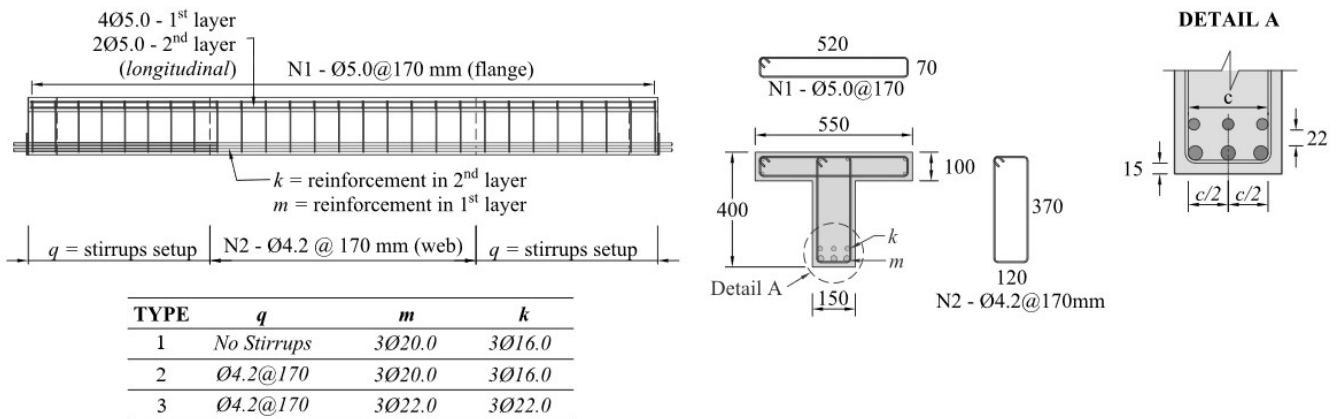


Figure 2 Internal steel reinforcement detailing for Types 1, 2, and 3 (dimensions in mm).

The transverse reinforcement in shear span consisted in vertical closed stirrups of Ø4.2@170mm for reinforcement types 2, and 3. Such a small diameter with elevated spacing were used to induce a shear failure, and simulate a deficient shear reinforcement. Type 1 reinforcement did not have stirrups in the shear span. Two different longitudinal reinforcement ratios were used: 3Ø20.0+3 Ø16.0 mm (1<sup>st</sup> and 2<sup>nd</sup> layers, respectively) ( $\rho = 1.54\%$ ), and 3Ø22+3Ø22 mm ( $\rho = 2.3\%$ ), the former for types 1, and 2, and the later for type 3. The types 2 and 3 differed only in the longitudinal reinforcement ratio. All reinforcement types had Ø5.0@170 mm stirrups and 4Ø5+2Ø5 mm longitudinal bars in the flange. Anchorage plates of 150x150x12.5 mm<sup>3</sup> thickness were used in tensile longitudinal bars to prevent slippage (Figure 1).

### 2.3 FRP strengthening schemes

The beams were strengthened with externally bonded FRP sheets cured in place in a U-shaped or in a fully-wrapped configuration. The five different arrangements differed in the FRP layout (spacing, thickness, and orientation), and anchorage type as schematically shown in Figure 3. In all schemes the strips were 150 mm wide perpendicular to fibers direction. The sharp edges of beam’s web were smoothed with a radius of 10 mm.

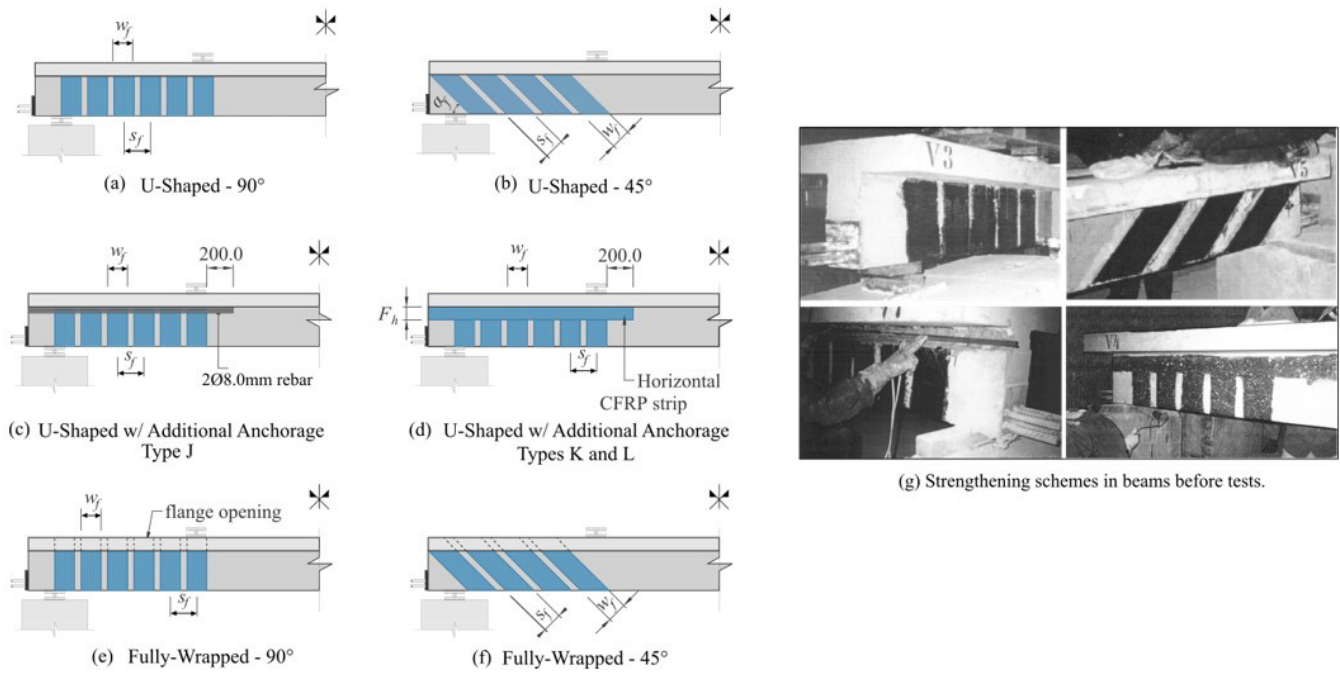


Figure 3 FRP strengthening types (dimensions in mm).

The U-shaped external strengthening system consisted of discontinuous FRP sheets at 45° or 90°, and up to three layers of FRP per strip. In addition, for this configuration, three different anchorages strategies were adopted in some beams, aiming to enhance FRP efficiency by delaying or preventing debonding to occur. Type J anchorage mechanism consisted of 2  $\varnothing$  8 mm bars mounted inside a groove in the web just beneath the flange, fixed with epoxy-based resin (Figure 3.c). Type K and L anchorages (Figure 3.d) consisted of a horizontal FRP strip placed parallel and close to the bottom face of the flange, which was mounted over the web FRP sheets. The difference between Type II and III anchorages was the strip width, being  $F_h=50$  mm, and  $F_h=100$  mm, respectively.

Finally, the fully-wrapped configuration is presented in Figures 3.e-f. In this case, the FRP sheets completely involved the web through openings made in the flange, which were filled after the FRP installation with repairing mortar, and coarse aggregate. The sharp edges of the web were smoothed with a fillet radius of approximately  $R=10$  mm for all specimens, aiming to reduce stress concentration, and premature FRP rupture.

## 2.4 Identification of the beams

The notation adopted to identify the specimen's is formatted as XX-YY-WWW-Z, with the following information:

- **XX**: series (A, B, or C), and sequence number (1 to 8);
- **YY**: reinforcement type (1, 2, or 3), and *P* for a pre-cracked beam;
- **WWW**: type (R, U or W, for reference beam, U-shaped or fully-wrapped, respectively), orientation (45 or 90°), and anchorage type (J, K, or L);
- **Z**: the number of FRP layers per strip (1, 2, or 3);

For instance, B8-2P-U90J-1 is the 8<sup>th</sup> beam from B series, with reinforcement type 2, which has been pre-cracked before applying the FRP, U-shaped scheme with type J anchorage, and fibers at 90°, and 2 layers of FRP per strip. In the text, the specimens can be also referenced in a short form only by its series and sequence number, i.e., B8. Table 1 summarizes the characteristics of the tested beams.

## 2.5 Material Properties

The mechanical properties of concrete were determined through testing cylindrical specimens, which measured 150 mm in diameter and 300 mm in height. The target concrete compressive strength was 30 MPa, and the mean strengths values (averaged from 10 specimens for each beam) on the test day are summarized in Table 1, ranging from 22.5 to 46.6 MPa. The tensile strengths were obtained via splitting tests on cylindrical specimens of the same dimensions. The values for tensile strength in Table 1 also represent the mean strength from 10 specimens for each beam.

**Table 1** Beam’s characteristics, and concrete strength.

Type	Beam	Fig.	Reinf. Type	Pre-Cracked	$\alpha_f$	Additional Anchorage	FRP Layers, $n_f$	FRP Spacing, $s_f$ (mm)	$f_c$ (MPa)	$f_{ct}$ (MPa)
Reference	A1-1-R	-	1	No	-	-	-	-	31.0	3.7
	A4-2-R	-	2	No	-	-	-	-	31.0	3.7
	B1-2-R	-	2	No	-	-	-	-	44.8	3.5
	C1-2-R	-	2	No	-	-	-	-	23.3*	2.2
	C5-3-R	-	3	No	-	-	-	-	46.1	3.1
U-Shaped	A2-1-U90-1	4.3.b	1	No	90°	-	1	230	44.6	3.5
	A3-1-U45-1	4.3.a	1	No	45°	-	1	230	44.6	3.5
	A5-2P-U90-1	4.3.b	2	Yes	90°	-	1	230	40.0	4.0
	A6-2P-U90-2	4.3.b	2	Yes	90°	-	2	200	40.0	4.0
	A7-2P-U45-1	4.3.a	2	Yes	45°	-	1	230	40.0	4.0
	A8-2P-U45-1	4.3.a	2	Yes	45°	-	1	180	40.0	4.0
	B4-2P-U90-3	4.3.b	2	Yes	90°	-	3	200	43.8	2.8
	U-Shaped with additional anchorage	B7-2P-U90J-1	4.3.c	2	Yes	90°	Type J	1	230	45.3
B8-2P-U90J-2		4.3.c	2	Yes	90°	Type J	2	200	45.3	3.0
C2-2P-U90K-1		4.3.d	2	Yes	90°	Type K	1	230	22.5*	2.0
C3-2P-U90L-1		4.3.d	2	Yes	90°	Type L	1	200	22.5*	2.0
C4-2P-U90L-2		4.3.d	2	Yes	90°	Type L	2	200	22.5*	2.0
Fully-wrapped	B2-2P-F90-1	4.3.e	2	Yes	90°	-	1	230	41.9	3.7
	B3-2P-F90-2	4.3.e	2	Yes	90°	-	2	200	42.2	3.1
	B5-2P-F45-1	4.3.f	2	Yes	45°	-	1	230	45.3	3.9
	B6-2P-F45-1	4.3.f	2	Yes	45°	-	1	200	46.4	3.5
	C6-3P-F90-1	4.3.e	3	Yes	90°	-	1	230	45.7	4.0
	C7-3P-F90-2	4.3.e	3	Yes	90°	-	2	200	45.8	3.1
	C8-3P-F45-1	4.3.f	3	Yes	45°	-	1	230	46.6	3.6

\* Concrete compressive strength lower than specified. -  $f_c$  and  $f_{ct}$  are test day values. Note: For all FRP sheets  $w_f=150$  mm.

The internal steel reinforcement had a nominal yield strength of 600 MPa for bars with diameters 4.2, and 5 mm, and 500 MPa for bars with 16-, 20-, and 22 mm diameters. The steel properties obtained from tensile tests are presented in Table 2. The minimum observed yielding strain in the 4.2 mm bars were  $\epsilon_{y_v}=0.0037$  mm/mm, and used as criteria for stirrups yielding. The Young’s Modulus was approximately 200 GPa.

**Table 2** Mechanical properties of the longitudinal, and transverse steel reinforcement obtained from tests.

$\varnothing$ (mm)	A Series			B Series			C Series		
	$f_{sy}$ (MPa)	$f_u$ (MPa)	$\epsilon_{sy}$ (mm/mm)	$f_{sy}$ (MPa)	$f_{su}$ (MPa)	$\epsilon_{sy}$ (mm/mm)	$f_{sy}$ (MPa)	$f_{su}$ (MPa)	$\epsilon_{sy}$ (mm/mm)
4.2	773	812	0.0057	769	808	0.0057	771	810	0.0043
5.0	781	843	0.0059	770	935	0.0046	886	929	0.0054
8.0	-	-	-	684	769	0.0052	-	-	-
16.0	619	755	0.0050	589	604	0.0047	656	820	0.0047
20.0	568	648	0.0047	620	705	0.0045	765	820	0.0053
22.0	-	-	-	-	-	-	712	841	0.0052

The FRP strengthening were applied by a wet lay-up system with unidirectional carbon fibers sheets and epoxy resin as the matrix. The application procedures followed the manufacturer’s recommendations, and the mechanical properties provided by them are summarized in Table 3.

**Table 3** Mechanical properties of FRP fibers provided by the manufacturer.

FRP Properties			
$t_f$ (mm)	$f_{fu}$ (MPa)	$E_f$ (GPa)	$\epsilon_{fu}$
0.165	3790	228	0.017

### 2.6 Instrumentation

The vertical displacements were measured at the load application points and at mid-span at the bottom side of the beams using dial gauges. An additional dial gauge was placed at the left end of the beam to measure its horizontal displacements. The dial gauges that were placed below the beam were removed before the last load step to prevent damage.

Strains in concrete were measured using strain gauges externally bonded to the upper face of the flange, specifically at the mid-span. The strain gauges were placed at mid-span and close to supports for the tensile reinforcement. The FRP strips' strains were measured with a single strain gauge per strip, located at mid-depth of the web. Due to the different strengthening schemes adopted, the second, third and fourth strips of FRP, counting from support toward the beam's mid-span, were chosen to be monitored. Within the shear span, three stirrups had two strain gauges at its mid-depth on each leg, and they were chosen in order to coincide with the FRP strips monitored. Figure 4 presents the position of strain gauges and dial-gauges.

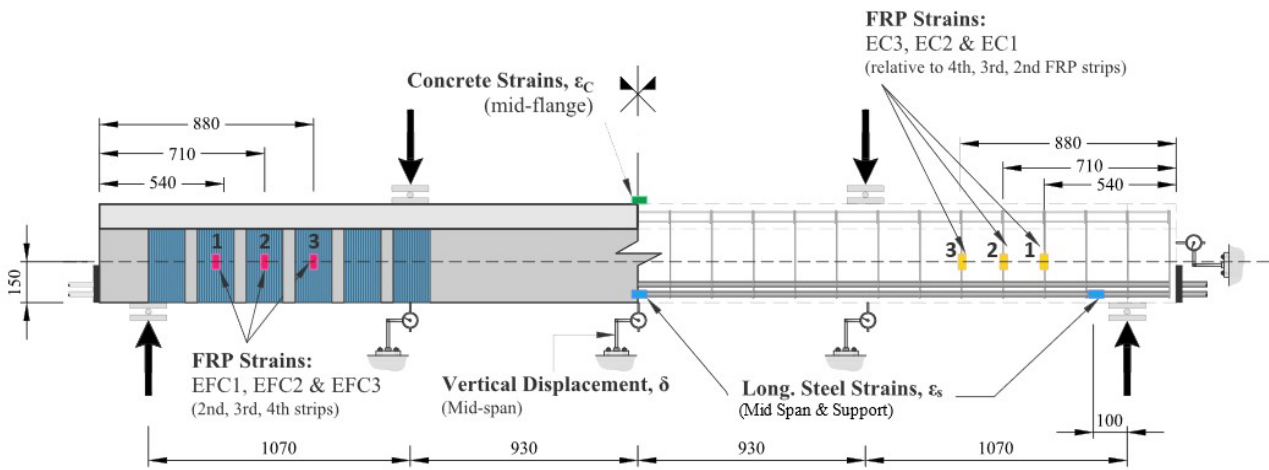


**Figure 4** Schematic representation of test configuration and instrumentation (dimensions in mm).

### 2.7 Testing

To replicate real-world conditions, the strengthened beams were previously loaded (Phase I) to ensure that they developed cracks before being strengthened with FRP sheets. Subsequently, these beams were subjected to testing until failure (Phase II) (as detailed in Table 1). During the pre-cracking tests (Phase I), for Type 2 reinforcement specimens in A and B series, the pre-cracking load level was 200 kN. For type 2 and 3 reinforcements in C series, the pre-cracking load levels were 150 kN and 225 kN, respectively. At this stage, the controlled shear crack widths on the beams were approximately to 0.3 mm, and the strain at the stirrups was 0.0024 mm/mm (below yielding point, see Section 2.5). Between Phase I and II, the beams underwent shear-strengthening using FRP sheets.

## 3 EXPERIMENTAL RESULTS

This section presents the primary experimental results. However, due to the abundance of experimental data, which includes sensor data, additional material properties, and pre-cracking testing, some of these results are not included in this paper and can be found in details in Salles Neto (2000), Silva Filho (2001) and Araújo (2002).

### 3.1 Shear strength and failure modes

Table 4 presents the experimental results in terms of experimental shear force close to the supports. The following key parameters are presented: the maximum shear force ( $V_{u,exp}$ ), the increment in shear capacity due to FRP ( $\Delta V$ ), the shear force at debonding initiation ( $V_{db}$ ), the shear force at stirrup yielding initiation ( $V_y$ ), the maximum displacement observed at mid-span ( $\delta$ ), and the shear force at longitudinal reinforcement yielding ( $V_{y,long}$ ). Additionally, the failure modes are documented.

**Table 4** Summary of the experimental results.

Type	Beam	$f_c$ (MPa)	$V_{db}$ (kN)	$V_y$ (kN)	$V_{u,exp}$ (kN)	$\Delta V$ (kN)	$\Delta V$ (%)	$\delta$ (mm)	$V_{y,long}$ (kN)	Failure Mode
Reference	A1-1-R	31.0	-	-	125.5	-	-	17.7	-	Shear
	A4-2-R	31.0	-	120	184.0	-	-	20.0	-	
	B1-2-R	44.8	-	175	180.0	-	-	19.5	-	
	C1-2-R	23.3	-	100	130.0	-	-	16.0	-	
	C5-3-R	46.1	-	140	186.0	-	-	15.7	-	
U-Shaped	A2-1-U90-1	44.6	130	-	138.0	12.5	10.0	12.3	-	Shear with FRP debonding
	A3-1-U45-1	44.6	130	-	160.0	34.5	27.5	16.1	-	
	A5-2P-U90-1	40.0	160	170	201.5	17.5	9.5	21.3	-	
	A6-2P-U90-2	40.0	180	***	201.5	17.5	9.5	20.2	-	
	A7-2P-U45-1	40.0	170	185	201.5	17.5	9.5	22.9	-	
	A8-2P-U45-1	40.0	160	***	197.5	13.5	7.3	18.9	-	
	B4-2P-U90-3	43.8	200	***	210.0	30.0	16.7	24.6	-	
U-Shaped with Additional anchorage	B7-2P-U90J-1	45.3	160	***	245.5	65.5	36.4	24.7	-	Shear with FRP debonding, and detachment of anchorage
	B8-2P-U90J-2	45.3	-	+	255.0	75.0	41.7	23.7	-	
	C2-2P-U90K-1	22.5	100	***	147.5	17.5	13.5	15.9	-	Shear with FRP debonding, and detachment of anchorage**
	C3-2P-U90L-1	22.5	150	***	157.5	27.5	21.2	16.8	-	
	C4-2P-U90L-2	22.5	145	***	150.0	20.0	15.4	15.0	-	
Fully-wrapped	B2-2P-F90-1	41.9	-	***	294.5	114.5	63.6	39.8	260	Flexure*
	B3-2P-F90-2	42.2	-	***	285.0	105.0	58.3	41.3	+	
	B5-2P-F45-1	45.3	-	***	289.5	109.5	60.8	44.1	258	
	B6-2P-F45-1	46.4	-	+	286.8	106.8	59.3	44.8	+	
	C6-3P-F90-1	45.7	209 <sup>1</sup>	285	325.0	139.0	74.7	26.7	-	Shear with FRP rupture
	C7-3P-F90-2	45.8	305 <sup>1</sup>	325	394.0	208.0	111.8	30.0	-	
	C8-3P-F45-1	46.6	265 <sup>1</sup>	265	306.0	120.0	64.5	22.1	-	

\*Flexure: yielding of longitudinal reinforcement with large crack width, followed by crushing of compressed concrete. \*\* Debonding of the anchorage horizontal strips followed by debonding of the vertical strips. \*\*\* No yielding observed in stirrups. + No data recorded due strain gauge premature failure.  
<sup>1</sup>Start of FRP debonding without rupture.

The results indicate that all strengthened beams exhibited an increase in the shear capacity. The predominant failure mode in the beams with U-shaped configuration was shear failure with FRP debonding, followed by anchorage detachment when present (beams B7, B8, C2-C4, for instance). Meanwhile, in beams with fully-wrapped scheme, failures were observed due to shear and flexure. For beams with less longitudinal reinforcement (beams B2, B3, B5, and B6), strengthening led to a change in the failure mode from shear to flexure. However, when a higher longitudinal reinforcement ratio was used (beams C6, C7, and C8), failure occurred by shear with rupture of FRP.

In the context of U-shaped beams without additional anchorage, the most substantial relative increment in shear capacity occurred in beam A3-1-U45-1, without stirrups in shear span, reaching 27.5% (34.5 kN). Among the beams with stirrups in shear span, beam B4-2P-U90-3, featuring three layers of FRP per strip, demonstrated a significant relative increase in shear capacity of 16.7% (30 kN). Conversely, beam A5-2P-U90-1, which differed from B4-2P-U90-3 by having only one FRP layer per strip, exhibited a 9.5% (17.5 kN) in shear capacity.

The results indicate that the increase in shear capacity for U-shaped strengthened beams is not direct proportional to the thickness of the FRP strip. Since debonding of the FRP is the predominant failure mode, increasing the strip thickness does not necessarily enhance the contact area between the FRP and the concrete – critical for adhesion and, consequently, the maximum force the FRP strip can withstand. Furthermore, the strength increment observed in the beam without stirrups (A3-1-U45-1) exceeded that of the equivalent beam with stirrups (A7-2P-U45-1), with relative increases of 27.5% (34.5 kN) and 9.5% (17.5 kN), respectively.

Only two beams strengthened in a U-shaped configuration (A5-2P-U90-1 and A7-2P-U45-1) exhibited stirrups yielding. In both cases, yielding was observed after the start of FRP debonding.

The additional anchorage significantly enhanced the shear capacity when compared to beams without it. The most substantial increments were observed in beams B8-2P-U90J-2 (41.7% and 75 kN) and B7-2P-U90J-1 (36.4% and 65.6 kN), both featuring Type J additional anchorage (2Ø8.0 mm). Notably, these increments were approximately four times greater than those observed in similar beams without additional anchorage, providing strong evidence of its efficiency.

The fully-wrapped configuration proved to be the most efficient type of strengthening, resulting in the highest increments of shear capacity. As already mentioned, some of these beams experienced failure due to flexure. Among those beams, the strengthening was particularly effective in beam B2-2P-F90-1, which exhibited a 63.6% (114.5 kN) increase in shear capacity. However, when the double the amount of FRP was applied to beam B3-2P-F90-2, the increment in shear capacity was slightly less, at 58.3% (105 kN). It's worth mentioning that in both cases, the strengthening successfully altered the failure mode from shear to flexure.

For the beams that failed in shear, the beam C7-3P-F90-2 exhibited the highest increase, at 111.8% (208 kN). It's worth mentioning that this beam has a higher longitudinal reinforcement ratio (Type 3) and a higher strengthening ratio (2 layers of FRP at 200 mm). The failure mode was shear, followed by FRP rupture, with yielding of stirrups in all beams within this group.

Figures 5 to 7 presents examples of the aspect of the beams after the testing, evidencing the crack patterns and FRP failure modes.

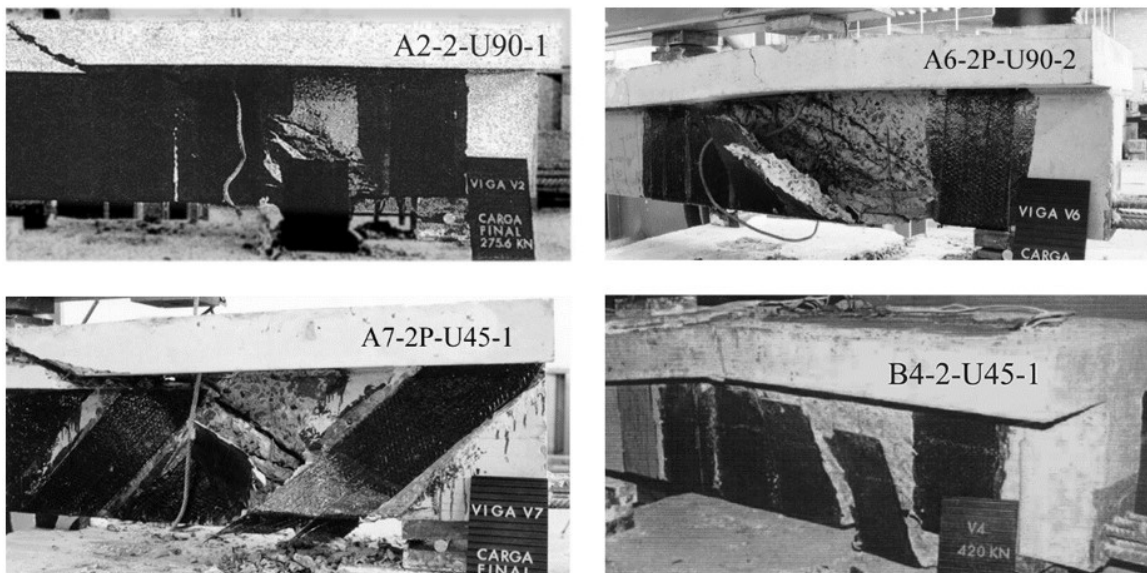


Figure 5 Examples of aspect of the beams with U-shaped configuration after testing.

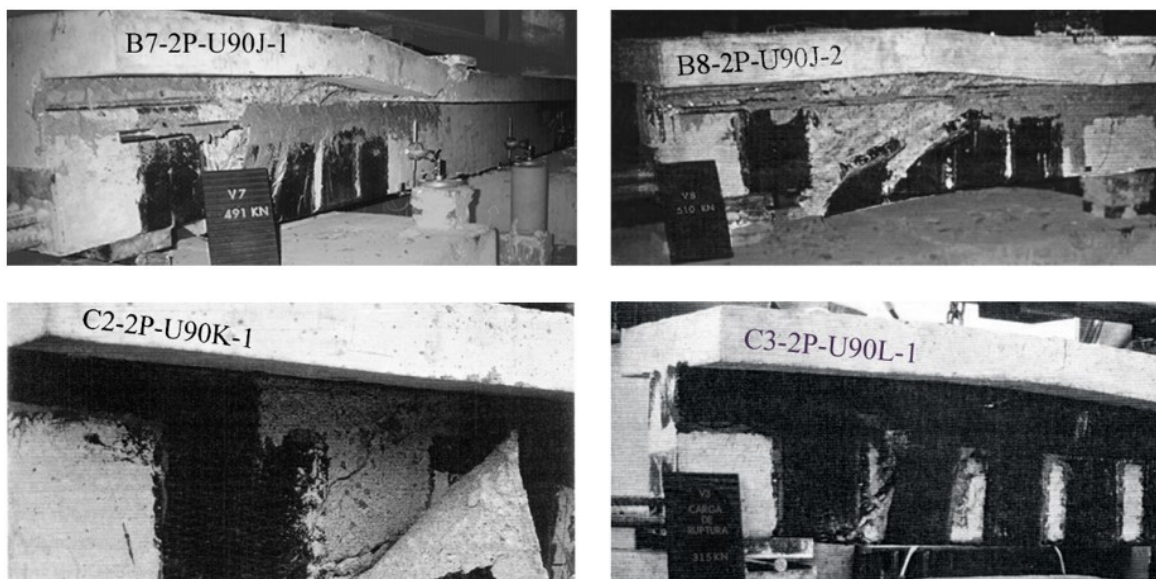


Figure 6 Examples of aspect of the beams with U-shaped configuration with additional anchorage after testing.

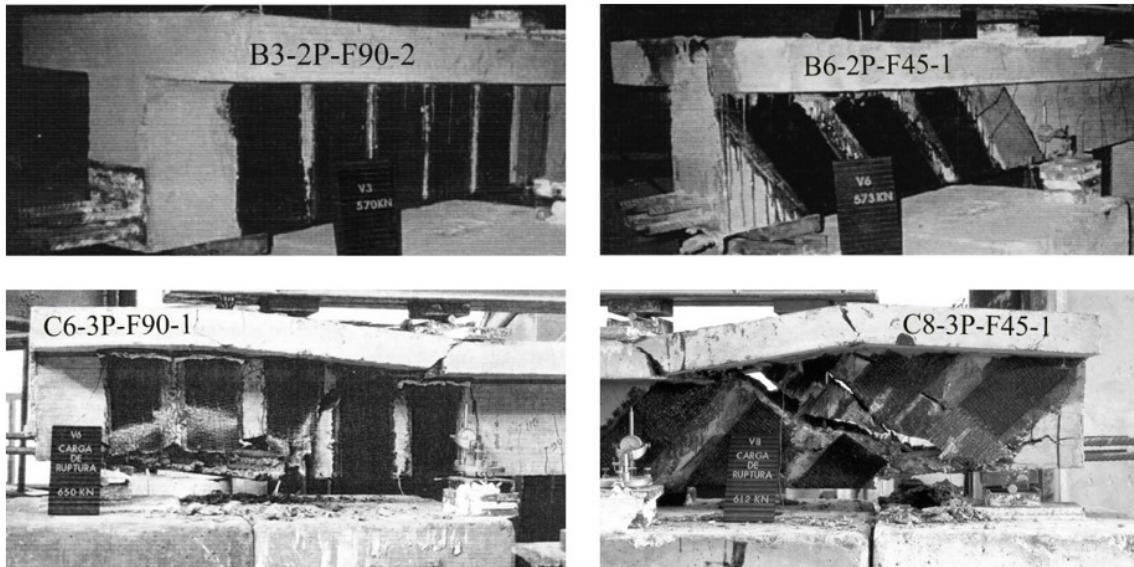


Figure 7 Examples of aspect of the beams with fully-wrapped configuration after testing.

### 3.2 Shear force-displacement

The shear force-displacement evolution for the reference beams is presented in Figure 8. One can see that, as expected, the shear strength for the beams without stirrups (Type 1 reinforcement) are lower than the ones with stirrups.

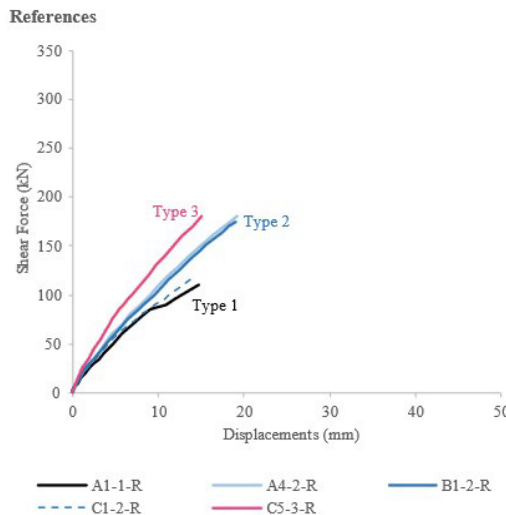


Figure 8 Shear force-displacement at mid-span behavior for reference beams.

In the context of beams strengthened with U-shaped FRP, two distinct behaviors can be observed (as shown in Figure 9). Although both exhibit similar stiffness, the beams without stirrups demonstrated a significant increase in shear capacity. However, the beams with stirrups showed shear capacity comparable to their reference beams. This behavior which can be attributed to the early debonding of the FRP strengthening.

The beams strengthened with U-shaped FRP and additional anchorages exhibited a significant increase in shear capacity when compared with those without additional anchorage, and their behavior is shown in Figure 10. The type J additional anchorage demonstrated to be more effective in delaying the debonding of FRP, which produced a higher increase in shear strength for the beams with it. The types K and L presented a similar behavior were and both capable of delaying FRP debonding. However, they were less effective than the type J.

The beams strengthened in a full-wrapped configuration exhibited two distinct failure modes. Beams with less longitudinal reinforcement (Type 2) displayed a classic ductile behavior, characterized by a plateau due to longitudinal reinforcement yielding. On the other hand, beams with higher longitudinal reinforcement ratio (Type 3) demonstrated a fragile failure mode involving shear and FRP failure. In both cases, the FRP strengthening was effective in highly increasing the shear capacity as shown in Figure 11.

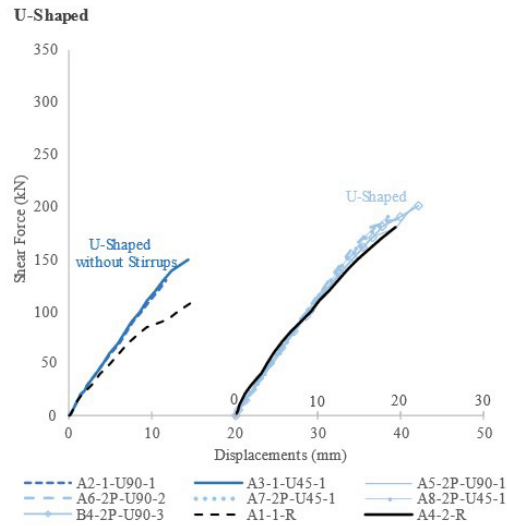


Figure 9 Shear force-displacement at mid-span behavior for beams strengthened with U-shaped FRP.

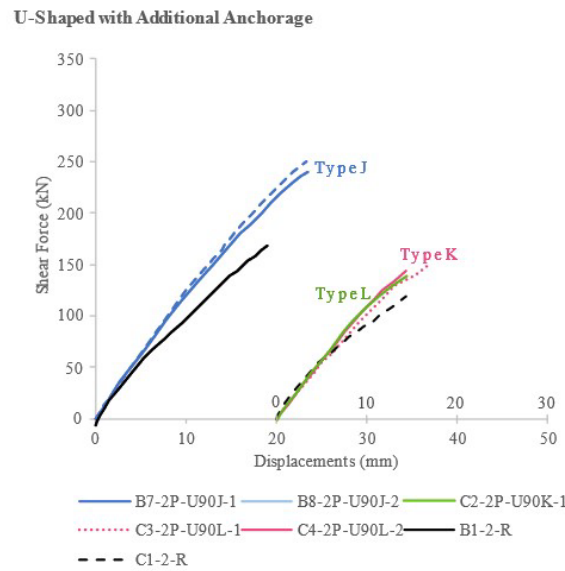


Figure 10 Shear force-displacement at mid-span behavior for beams strengthened with U-shaped FRP and additional anchorage.

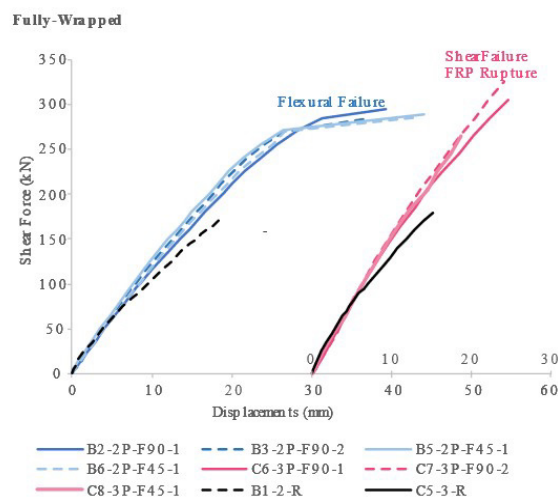


Figure 11 Shear force-displacement at mid-span behavior for beams strengthened in fully-wrapped configuration.

### 3.3 Strains in stirrups and FRP

Figure 12 depicts a comparison between similar beams strengthened using a U-shaped scheme, varying in the presence or absence of stirrups and number of layers per FRP strips. Stirrups yielded only in beam A5-2P-U90-1. However, strains in both stirrups and FRP were comparable to those in beam B4-2P-U90-3, which had three FRP layers per strip. The maximum observed strain in FRP was 0.4%, and it was similar among the three beams. However, for A5-2P-U90-1, after debonding was noticed in one FRP strip, the adjacent strip was activated, and a sudden increase in strains for this strip can be observed in Figure 12. Meanwhile, beam B4-2P-U90-3 as well as A2-1-U90-1 failed after debonding of the first strip.

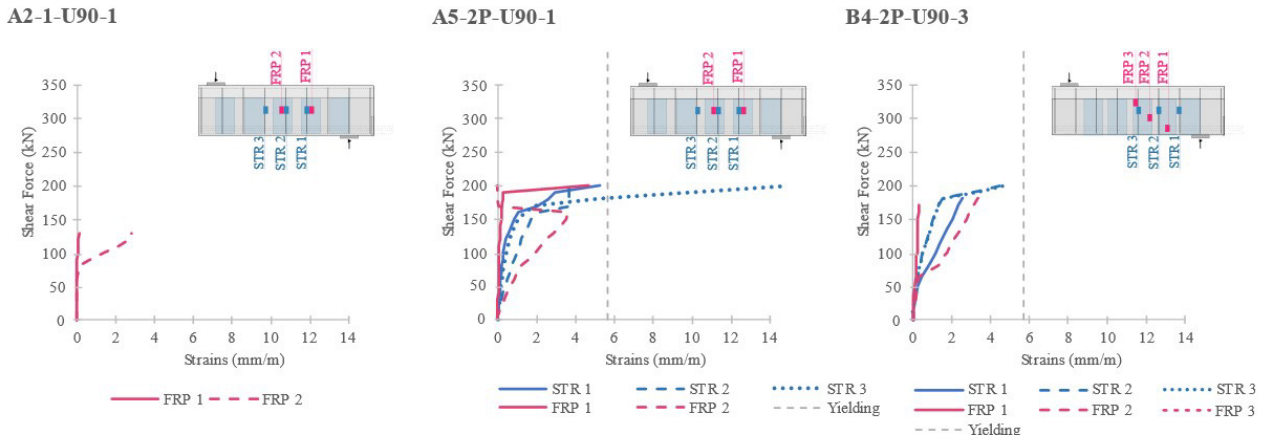


Figure 12 Strains in FRP and stirrups for beams in a U-shaped strengthening configuration.

Among the beams strengthened in a U-shaped scheme with additional anchorage, beam B7-2P-U90J-1 with Type J additional anchorage exhibited higher strain levels than those with Type K and L, as well as the beams without additional anchorage (see Figure 13). This provides evidence of the influence of additional anchorage and its superior efficiency of compared with the other types. Notably, the FRP strain levels were up to 2.5 higher in beam B7-2P-U90J-1.

The beams in a fully-wrapped strengthening scheme exhibited lower strain levels when the observed failure mode was due to flexure (see Figure 14). In these beams, the strains levels for stirrups and FRP were closely related. Additionally, beam B3-2P-F90-2, which had twice the amount of FRP compared to B2-2P-F90-1, showed lower strain levels than the later.

Finally, the similarity between strain levels for stirrups and FRP was observed in beams with a fully-wrapped scheme and that failed in shear (see Figure 15). Furthermore, strain levels in beam C7-3P-F90-2 were lower than those in beam C6-3P-F90-1 for an equivalent shear force level. Those beams differ only by the amount of FRP, which is higher in the former. The lower strain levels for FRP in beam C7-3P-F90-2 is evidence that increasing the amount of FRP make it stiffer and limits its stretching. A comparable behavior was noticed in beams C6-3P-F90-1 and C8-3P-F45-1, which differ only in FRP orientation, and presented a slightly higher shear capacity than beam C6-3P-F90-1.

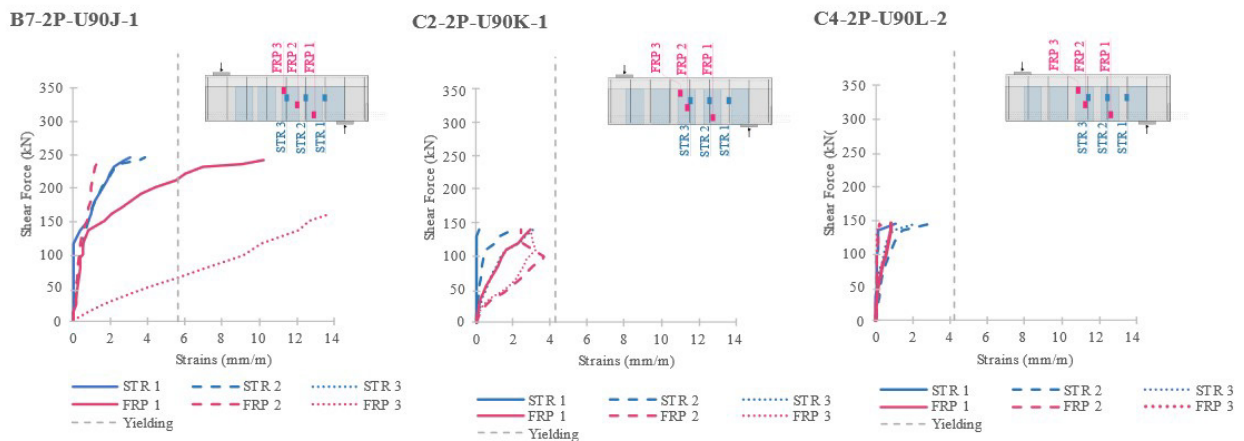


Figure 13 Strains in FRP and stirrups for beams in a U-shaped strengthening configuration with additional anchorage.

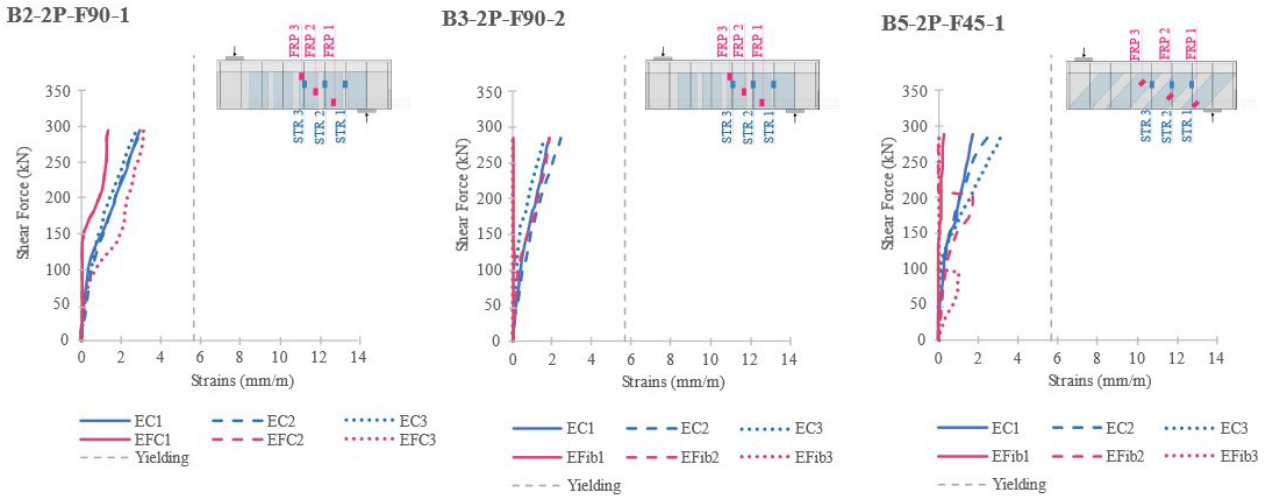


Figure 14 Strains in FRP and stirrups for beams in a fully-wrapped scheme and flexural failure.

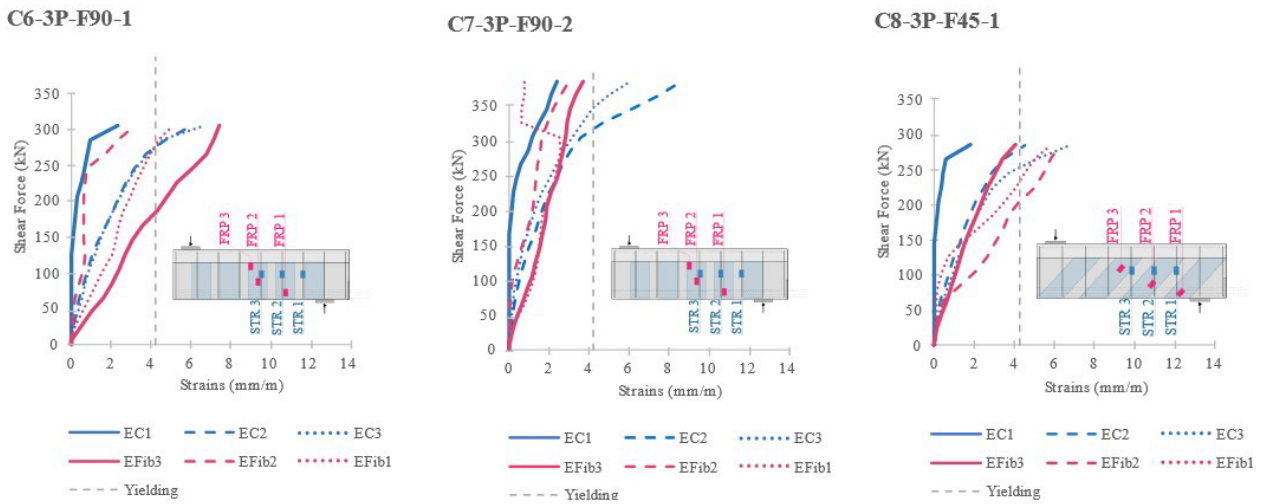


Figure 15 Strains in FRP and stirrups for beams in a fully-wrapped scheme and shear failure.

### 4 CONTRIBUTIONS TO SHEAR STRENGTH

In this section, the contributions to shear strength from FRP and stirrups are estimated based on experimental strain data. The methodology employed is derived from the work of Oller, Pujol and Marí (2019) and Autrup, Jørgensen and Hoang (2022). The following assumption is made: shear strength can be approximated as shear resistance due to stirrups and FRP intersected by the shear crack that leads to beam failure. Additionally, the complementary truss mechanism is embedded in the concrete contribution. It is estimated as the difference between the total shear strength and the sum of contributions from FRP and stirrups, as in the following,

An additional approximation is to consider that only the FRP and stirrups monitored contribute to shear strength, and that the measured strain is representative for the entire element (FRP or stirrup). It is well-known that the strains at the intersection with shear crack can be higher than the measured ones. However, it is impractical to predict the shear crack precisely, and the assumptions made here can be seen as conservative for FRP and stirrups.

Based on these assumptions, the shear contribution from stirrups can be estimated assuming a bilinear elastoplastic stress-strain behavior. Using measured strains and a constitutive law, the stresses can be estimated, and consequently, the shear contribution is estimated as the vertical component of the resulting force in the stirrups. Similarly, the shear contribution from FRP can be estimated as the vertical component of the resulting force, assuming a linear-elastic behavior between stresses and strains. It is also assumed that the stresses are uniform within the cross-section.

The summary of results for the instant where the maximum combined shear contribution from stirrups and FRP are observed are shown in Table 5.

**Table 5** Summary of shear contribution at the instant of maximum combined contribution of FRP and stirrups.

Type	Beam	$V_{u,exp}$ kN	$V_w(V_s+V_f)_{max}$ kN	$(V_s+V_f)_{max}$ kN	$V_s$		$V_f$		$V_c$		$\epsilon_{f,max}$ mm/m
					kN	%	kN	%	kN	%	
U-shaped	A2-1-U90-1	138.0	130	33.6	-	-	33.6	26	96.4	74	2.85
	A3-1-U45-1	160.0	150	40.1	-	-	40.1	27	109.9	73	4.41
	A5-2P-U90-1	201.5	200	117.1	64.3	32	52.8	26	82.9	41	4.68
	A6-2P-U90-2	201.5	180	84.1	15.8	9	68.3	38	95.9	53	2.93
	A7-2P-U45-1	201.5	170	73.9	37.7	22	36.2	21	96.1	57	4.08
	A8-2P-U45-1	197.5	180	61.1	35.5	20	25.6	14	118.9	66	3.19
	B4-2P-U90-3	210.0	170.8	148.4	30.4	18	118.0	69	22.4	13	3.37
U-shaped with additional anchorage	B7-2P-U90J-1	245.5	240	182.0	58.5	24	123.5	51	58.0	24	13.90
	B8-2P-U90J-2	255.0	*	*	*	*	*	*	*	*	*
	C2-2P-U90K-1	147.5	140	93.1	30.1	21	63.0	45	46.9	34	3.70
	C3-2P-U90L-1	157.5	150	70.7	23.9	16	46.7	31	79.3	53	2.81
	C4-2P-U90L-2	150.0	145	61.1	36.4	25	24.7	17	83.9	58	0.84
Fully-wrapped	B2-2P-F90-1	294.5	294.5	92.1	51.8	18	40.3	14	202.4	68	3.14
	B3-2P-F90-2	285.0	285	55.5	34.3	12	21.2	7	229.5	81	1.88
	B5-2P-F45-1	289.5	289.5	46.5	44.3	15	2.2	1	243.0	84	1.77
	B6-2P-F45-1	286.8	*	*	*	*	*	*	*	*	*
	C6-3P-F90-1	325.0	305	236.0	56.5	19	179.5	58	69.0	23	7.51
	C7-3P-F90-2	394.0	385	152.2	57.0	15	95.2	25	232.8	60	3.79
C8-3P-F45-1	306.0	285	313.0	53.0	19	260.0	91	-28.0	-10	6.31	

\*Insufficient experimental data.

By examining of Table 5, one can observe that beams with higher relative strength contribution from FRP exhibited a greater increase in shear capacity. Additionally, for well-anchored FRP configurations (such as fully-wrapped and Type J additional anchorage), the strain levels were superior to those observed in U-shaped configurations. Notably, beam C7-3P-F90-2, due to its larger amount of FRP, displayed lower strain levels and FRP contribution compared to beam C6-3P-F90-1, which had half the amount of FRP. A similar behavior was observed for beams A5-2P-U90-1 and B4-2P-U90-3, where the increased FRP content resulted in stiffer FRP and lower strains levels.

### 3.3 Influence of strengthening scheme

Table 6 presents a comparison between similar beams differing mainly by the strengthening configuration. The evolution of shear contribution for the same beams are shown in Figure 16.

**Table 6** Comparison of shear contribution and strengthening configuration.

Type	Beam	$f_c$	$f_{c,ref}$	$V_{u,ref}$	$V_u$	$\Delta V$		$V_s+V_f$		$V_s$		$V_f$		Failure Mode
		MPa	MPa	kN	kN	kN	%	kN	%	kN	%	kN	%	
U-shaped w/o stirrups	A2-1-U90-1	44.6	31.0	125.5	138.0	12.5	10.0	33.58	26	-	-	33.5	26	Shear with FRP debonding
U-shaped	A5-2P-U90-1	40.0	31.0	184.0	201.5	17.5	9.5	117	59	64.3	32	52.8	26	
U-shaped with additional anchorage	B7-2P-U90J-1	45.3	44.8	180.0	245.5	65.5	36.4	160.8	76	58	24	123.4	51	
Fully-wrapped	B2-2P-F90-1	41.9	44.8	180.0	294.5	114.5	63.6	92.2	28	51.8	18	30.1	10	Flexure
	C6-3P-F90-1	45.7	23.3	186.0	325.0	139.0	74.7	236.0	77	56.5	19	179.5	58	Shear with FRP rupture

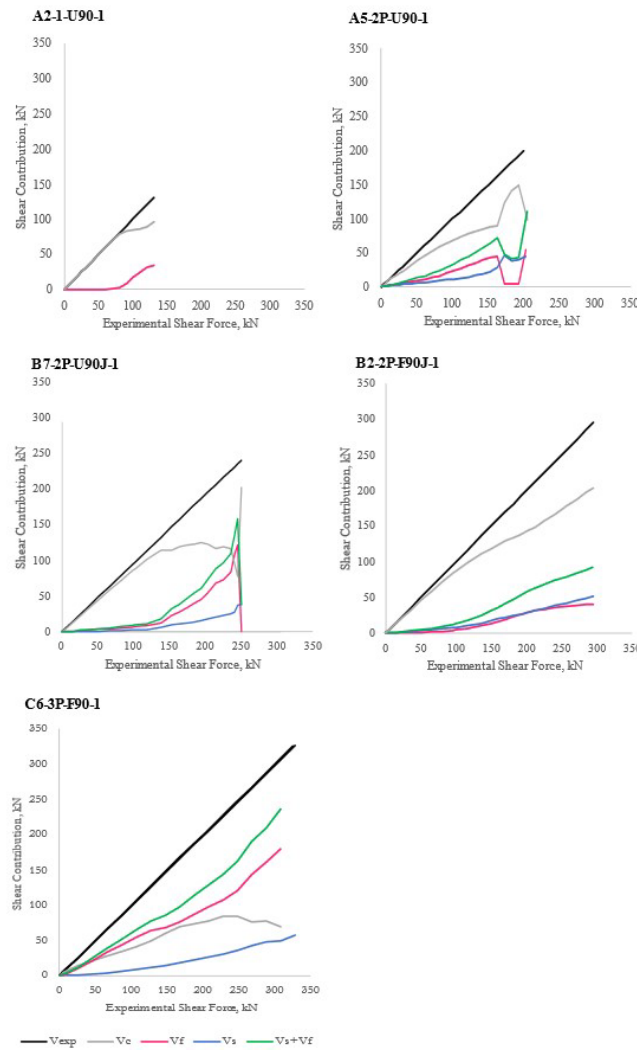


Figure 16 Shear contribution evolution with the internal shear force: a comparison between strengthening schemes.

Analyzing Table 6, it is evident that there is a correlation between the support type for FRP (no anchorage, additional anchorage, and fully-wrapped) and the increase in shear capacity. The FRP contribution exhibits a crescent behavior of 33.5 kN (26%), 52.8 kN (26%), 123.4 kN (51%), and 179.5 kN (58%), for U-shaped without and with stirrups, U-shaped with additional anchorage, and fully-wrapped that failed in shear, respectively. As a direct consequence, the joint contribution from FRP and stirrups also follows a crescent pattern, as depicted in Figure 16. The shear contribution from stirrups remains roughly constant across the different types of strengthening schemes. This provides further evidence of the influence of the strengthening scheme on the increase in shear capacity. In Figure 16, beam A5-2P-U90-1 exhibits an increase in stirrups contribution after the debonding of the first FRP strip (discontinuity in contribution of FRP). Afterwards, an adjacent strip of FRP is activated, and by the time it debonds, the failure occurs. In this case, the shear contribution for FRP was similar to those observed in beam A2-1-U90-1.

### 5 COMPARISONS BETWEEN EXPERIMENTAL RESULTS AND ANALYTICAL PREDICTION

This section compares the experimental results with those estimated by the ACI 440.2R (2017), fib Bulletin 90 (2019), and fib Bulletin 14 (2001) (see Appendix 1). These standards codes are well-established and provides an estimative of the FRP contribution, in addition to that coming from concrete and stirrups. For these models, the FRP contribution is considered to be the difference in shear capacity between the strengthened beam and a comparable one without FRP systems. consequently, these models do not consider any interaction between stirrups and FRP.

The ACI 440.2R assumes a 45° angle for the orientation of the shear crack, which is a conservative assumption, whereas fib Bulletins 14 and 90 allow this orientation to be arbitrarily chosen by the designer within certain limits. For the results presented in Table 7, the orientation of the shear crack was set at 45° in fib Bulletin 14 to facilitate a fair

comparison with ACI 440.2R. However, for fib Bulletin 90, three different angles for orientation of the shear crack were set. This strategy aims to explore the possibilities of it, as it is a recent model with limited presence in existing literature. In all cases, the safety coefficients were not considered. The results are summarized in Table 7, where the values between parenthesis are the theoretical-experimental ratio, i.e.  $\zeta = V_{f,exp}/V_{f,theor}$  and  $\zeta \leq 1$  represents the safe side.

In the case of U-shaped FRP strengthening, the predicted values range from 0.9 to 6.5 times the shear capacity observed in experimental campaign. Comparing the results for beams A5-2P-U90-1, A6-2P-U90-2, B4-2P-U90-3, which mainly differs by the number of FRP layers per strip, it is evident that the predicted  $V_f$  values are linearly related with the number of layers. This linearity is consistent across the theoretical models and may not reflect realistic outcomes. In beams strengthened with U-shaped FRP, the failure mode is often debonding, closely associated with the bond surface between the concrete and the FRP. Therefore, increasing FRP thickness may not be as beneficial as enlarging the bond area between concrete and FRP. The fib Bulletin 90 model yielded better numerical results on average for the increment of shear resistance despite not accurately predicting the correct failure mode for all beams, i.e., it predicted FRP rupture when debonding was observed in experimental tests.

The beams strengthened with U-shaped FRP with additional anchorage were considered as U-shaped for applying the theoretical models, which is a conservative assumption. Inspecting Table 7, one can see a slightly improvement in performance for the three models. The performance of ACI 440.2R and fib Bulletin 90 where similar, in an average sense, even though most of results are still on the unsafe side.

**Table 7** Comparison of experimental results and analytical models.

Type	Beam	$V_{exp}$ (kN)	$V_f = \Delta V$ (kN)	$V_f = \Delta V$ (%)	ACI 440.2R	fib Bul. 14	Fib Bul. 90
					$V_f$ (kN)	$V_f$ (kN)	$V_f$ (kN)
U-shaped	A2-1-U90-1	138	12,5	10	46.9 (3.8)	75.3 (6.0)	29.8 (2.4)
	A3-1-U45-1	160	34,5	27,5	46.9 (1.4)	91.4 (2.7)	29.8 (0.9)
	A5-2P-U90-1	201,5	17,5	9,5	46.9 (2.7)	72.3 (4.1)	30.0 (1.7)
	A6-2P-U90-2	201,5	17,5	9,5	88.0 (5.0)	98.1 (5.6)	68.9 (3.9)
	A7-2P-U45-1	201,5	17,5	9,5	46.9 (2.7)	87.8 (5.0)	30.0 (1.7)
	A8-2P-U45-1	197,5	13,5	7,3	60.0 (4.4)	87.8 (6.5)	38.3 (2.8)
	B4-2P-U90-3	210	30	16,7	107.9 (3.6)	117.2 (3.9)	103.5 (3.5)
	B7-2P-U90J-1	245,5	65,5	36,4	46.9 (0.7)	75.7 (1.2)	42.7 (0.7)
	B8-2P-U90J-2	255	75	41,7	95.6 (1.27)	58.3 (1.4)	98.3 (1.3)
	C2-2P-U90K-1	147,5	17,5	13,5	35.9 (2.0)	58.3 (3.3)	31.2 (1.8)
U-shaped with Additional Anchorage	C3-2P-U90L-1	157,5	27,5	21,2	41.3 (1.9)	58.3 (2.8)	35.9 (1.7)
	C4-2P-U90L-2	150	20	15,4	64,1 (3.9)	79.1 (5.1)	71.7 (4.7)
	B2-2P-F90-1	294,5	114,5	63,6	47.0 (0.7)	139.9 (2.2)	117.4 (1.8)
	B3-2P-F90-2	285	105	58,3	108.0 (1.9)	227.6 (3.9)	270.0 (4.6)
	B5-2P-F45-1	289,5	109,5	60,8	47.0 (0.8)	157.7 (2.6)	99.8 (1.6)
	B6-2P-F45-1	286,8	106,8	59,3	54.0 (0.9)	142.8 (2.4)	114.8 (1.9)
	C6-3P-F90-1	325	139	74,7	47.0 (0.6)	141.3 (1.9)	117.4 (1.6)
	C7-3P-F90-2	394	208	111,8	108.0 (1.0)	229.6 (2.1)	270.1 (2.4)
Fully-wrapped	C8-3P-F45-1	306	120	64,5	47.0 (0.7)	156.8 (2.4)	99.8 (1.5)

For beam with fully-wrapped FRP configuration, the superior results provided by the ACI 440.2R are evident, with all the predictions on the conservative side. A lower dispersion was observed in all three models, especially for the beams that failed in shear (C6, C7 and C8), offering the most accurate predictions among the different strengthening schemes.

## 6 CONCLUSIONS

This paper presented the results of an experimental campaign with 24 reinforced concrete beams, which 19 were strengthened in shear with externally bonded FRP systems. The main objectives were to investigate the influence of the strengthening configuration on the increase in shear capacity, strains in FRP and stirrups, and consequently, the FRP contribution to shear strength. By means of experimental data for strains, the contribution of FRP and stirrups in the shear span was estimated and its evolution with the total shear capacity presented. Based on the observations and results presented in this paper, the following conclusions can be made:

- The results presented in this paper demonstrated that the FRP contribution to shear strength is closely related to its straining capacity, which can be enhanced by providing an adequate anchorage;
- For the beams studied in U-shaped configuration, the increase in shear capacity was similar for beams with and without stirrups in shear span, despite of the amount of FRP per unit length. This suggests that the bond area between concrete and FRP plays a more significant role than the FRP thickness when debonding controls the failure. This inference is supported by the comparable results for beams differing mainly in the number of FRP layers per strip. For instance, comparing beams A5-2P-U90-1 (1 layer of FRP per strip) and B4-2P-U90-3 (3 layers of FRP per strip), the increase in shear capacity did not correlate with the amount of FRP per unit length, being of 17.5 (27.5 %) and 30 kN (16.7%), respectively. Furthermore, the beam A3-1-U45-1, which had a larger bond area between FRP and concrete when compared to A2-1-U90-1, showed a greater increase in shear capacity (27.5% and 10%, respectively) for the same spacing between successive FRP strips and number of layers per strip.
- Beams strengthened in shear with FRP in a U-shaped configuration and without stirrups in shear span exhibited a greater increase in shear capacity (both absolute and relative) than those with stirrups. This indicates an interaction between stirrups and FRP strengthening, warranting further investigation into this phenomenon and its impact on shear strength;
- Providing an anchorage to FRP strips can postpone the onset of debonding, allowing FRP to achieve higher strain levels and, consequently, a greater increase in shear capacity. Utilizing rebars as an anchorage system has been shown to increase the capacity of studied beams up to 41%. However, the use of horizontal strips were not as effective, and the beams strengthened with them exhibited a similar increase in shear capacity to those without additional anchorage, ranging from 17.5 to 27.5 kN;
- The fully-wrapped FRP configuration proved to be the most efficient strengthening method, yielding increases in shear capacity ranging from 105 to 208 kN, and from 58.3 to 111.8%. The results demonstrate that when FRP is properly anchored, it achieves superior strain levels, significantly enhancing its contribution to the overall shear capacity;
- The contribution to FRP shear capacity was estimated using ACI 440.2R, fib Bulletins 14 and 90. For the beams discussed in this paper, a high variance in results was observed, with a significant number of predictions falling on the unsafe side, particularly for U-shaped configurations.
- For U-shaped beams, the average performance was better for fib Bulletin 90. However, this code suggested an inaccurate failure mode, which did not align with experimental observations.
- A lower dispersion was noted for the fully-wrapped configuration, with ACI 440.2R providing the most accurate predictions.
- The models clearly indicate a linear relationship between the FRP thickness and the predicted shear contribution of FRP. Nonetheless, experimental findings suggest that increasing FRP thickness may be ineffective for U-shaped configurations when failure is due to debonding.
- Lastly, none of the models account for the interaction between FRP and stirrups, treating their shear contributions as independent, contrary of what experimental results imply. Developing strategies that consider this interaction could represent a significant advancement.

## ACKNOWLEDGEMENTS

The authors wish to express their gratitude to CAPES, CNPq and FAP-DF, Brazilian Research Development Agencies, for supporting the work described in this paper. The support of the University of Brasilia and of the Federal Institute of Ceará, and the tests being done by Alessandro S. Araújo, José N. Silva Filho and Moacyr Salles Neto are also acknowledged.

**Author's Contributions:** Conceptualization: Jonathas F. O. Iohanathan and Guilherme S. S. A. Melo; Methodology: Jonathas F. O. Iohanathan; and Guilherme S. S. A. Melo; Investigation: Jonathas F. O. Iohanathan and Guilherme S. S. A. Melo; Writing - original draft: Jonathas F. O. Iohanathan; Writing: Jonathas F. O. Iohanathan; Funding acquisition: Guilherme S. S. A. Melo; Resources: Guilherme S. S. A. Melo; Supervision: Guilherme S. S. A. Melo.

**Editor:** Marco L. Bittencourt

## References

- ACI Committee 440 (2017). ACI 440-2R-17: Guide for The Design and Construction of Externally Bonded FRP Systems for Strengthening Concrete Structures. American Concrete Institute. Farmington Hills, MI.
- Al-Saidy, A.H., Al-Harthy, A.S., Al-Jabri, K.S., Abdul-Halim, M., Al-Shidi, N.M. (2010). Structural performance of corroded RC beams repaired with CFRP sheets. *Composites Structures* 92:1931-1938.
- Araújo, A. S. (2002). T-Beams Strengthened in Shear with CFRP Laminates, Master Thesis (in Portuguese), University of Brasília.
- Autrup, F; Jørgensen, H. B.; Hoang, L. C., The influence of small amounts of shear reinforcement on the shear-transferring mechanisms in RC beams: An analysis based on refined experimental measurements, *Structural Journal*, 2022. DOI: <http://dx.doi.org/10.1002/suco.202200193>
- Autrup, F., Jørgensen, H. B., Hoang, L. C. (2023). The influence of small amounts of shear reinforcement on the shear-transferring mechanisms in RC beams: An analysis based on refined experimental measurements. *Structural Concrete* 24-2.
- Bousselham, A., Chaallal, O. (2006). Behaviour of RC T-beams strengthened in shear with CFRP: an experimental study. *ACI Structural Journal*.
- Chen, G. M., Li, S. W., Fernando, D., Liu, P. C., Chen, J. F. (2017). Full-range FRP failure behavior in RC beams shear-strengthened with FRP wraps. *International Journal of Solids and Structures* 125:1-21.
- Chen, G. M., Zhang, Z., Li, Y.L., Li, X.Q., Zhou, C.Y. (2016). T-section RC beams shear-strengthened with anchored CFRP U-strips. *Composite Structures* 144:57-79.
- Colotti, V. (2013). Shear interaction effect between transverse reinforcements in FRP-strengthened RC beams. *Composites Part B: Engineering* 45:1222-1233.
- Deniaud, C., Cheng, R.J.J. (2003). Reinforced concrete T-beams strengthened in shear with fiber reinforced polymer sheets. *Journal of Composites for Construction* 7:302-310.
- Monti, G., Liotta, M. (2007). Tests and design equations for FRP-strengthening in shear. *Construction and Building Materials* 21:799-809.
- National Research Council Advisory Committee on Technical Recommendations for Construction (2004). Guide for the Design and Construction of Externally Bonded FRP Systems for Strengthening Existing Structures, CNR-DT200.
- Fib (Fédération Internationale du Béton) (2001). Externally bonded FRP reinforcement for RC structures. *Fib Bulletin* 14.
- Fib (Fédération Internationale du Béton) (2019). Externally Applied FRP Reinforcement for Concrete Structures. *Fib Bulletin* 90.
- Fu, B., Tang, X.T., Li, L.J., Liu, F., Lin, G. (2018). Inclined FRP U-jackets for enhancing structural performance of FRP-plated RC beams suffering from IC debonding. *Composite Structures* 200: 36-46.
- German Committee for Reinforced Concrete. (2013). Erläuterungen und Beispiele zur DAfStb-Richtlinie Verstärken von Betonbauteilen mit geklebter Bewehrung (in German). Berlin. Germany. DAfStb Heft 595.

- Karzad, A.S., Leblouba, M., Toubat, S.A., Maalej, M. (2019). Repair and strengthening of shear-deficient reinforced concrete beams using Carbon Fiber Reinforced Polymer. *Composite Structures* 223.
- Khalifa, A., Nanni, A. (2000). Improving the shear capacity of existing RC T-section beams using CFRP composites. *Cement and Concrete Composites* 22:165-174.
- Li, W., Leung, C. K. Y. (2017). Effect of shear span-depth ratio on mechanical performance of RC beams strengthened in shear with U-wrapping FRP strips. *Composite Structures* 177:141-157.
- Oller, E.; Pujol, M.; and Mari, A. (2019). Contribution of externally bonded FRP shear reinforcement to the shear strength of RC beams. *Composites Part B* 164:235-248.
- Pellegrino, C., Modena, C. (2002). Fiber reinforced polymer shear strengthening for reinforced concrete beams with transverse steel reinforcement. *Journal of Composites for Construction* 6.
- Salles Neto, M. (2000). Behavior of "T" beams strengthened in shear with carbon sheet laminates (CFRP). Master Thesis (in Portuguese). University of Brasília.
- Siddika, A., Al-Mamun, M. A., Alyousef, R., Amran, Y.H.M. (2019). Strengthening of reinforced concrete beams by using fiber-reinforced polymer composites: A review. *Journal of Building Engineering* 25.
- Silva Filho J. N. (2001). Additional tests in "T" beams strengthened in shear with CFRP laminates. Master Thesis (in Portuguese). University of Brasília.
- Spinella, N. (2019). Modeling of shear behavior of reinforced concrete beams strengthened with FRP. *Composite Structures* 215:351-364.
- Yu, F., Guo, S., Wang, S., Fang, Y. (2019). Experimental study on high pre-cracked RC beams shear-strengthened with CFRP strips. *Composite Structures* 225.

**Appendix 1. Summary of equations to evaluate the FRP contribution to shear strength. Units are in SI (N, mm).**

ACI 440.2R (ACI Committee 440, 2017)

FRP contribution to shear strength	$V_f = \frac{A_f E_f \varepsilon_{fe} (\sin \alpha_f + \cos \alpha_f) d_f}{S_f}$	
	Where: $E_f$ : FRP Young's Modulus; $\alpha_f$ : FRP orientation with the longitudinal axis of the beam; $d_f$ : Effective depth of the FRP shear reinforcement; $A_f$ : area of FRP shear reinforcement;	
Effective strain in FRP, $\varepsilon_{fe}$	$\varepsilon_{fe} = 0.004 \leq 0.75 \varepsilon_{fu}$	For fully-wrapped schemes
	$\varepsilon_{fe} = k_v \varepsilon_{fu}$	For U-shaped or side-bonded FRP
Ultimate FRP strain, $\varepsilon_{fu}$	$\varepsilon_{fu} = C_E \varepsilon_{fu}^*$	
	Where: $C_E$ : environmental reduction factor $\varepsilon_{fu}^*$ : ultimate rupture strain of FRP reinforcement	
Bond reduction coefficient, $k_v$	$k_v = \frac{k_1 k_2 L_e}{11900 \varepsilon_{fu}} \leq 0.75$	
	With: $k_1 = \left( \frac{f_{ck}}{27} \right)^{2/3}$ $k_2 = \begin{cases} \frac{d_f - L_e}{d_f}, & \text{For U - jacketing} \\ \frac{d_f - 2L_e}{d_f}, & \text{For side bonding} \end{cases}$	
Active bond length, $L_e$	$L_e = \frac{23300}{(n_f t_f E_f)^{0.58}}$	

Fib Bulletin 14 (Fib, 2001)

FRP contribution to shear strength	$V_{fd} = 0.9 \varepsilon_{fd,e} E_f \rho_f b_w d (\cot \theta + \cot \alpha) \sin \alpha$	
Design value of effective strain in FRP, $\varepsilon_{fd,e}$	$\varepsilon_{fd,e} = \frac{0.8 \varepsilon_{f,e}}{\gamma_f}$	
Effective strain for FRP, $\varepsilon_{f,e}$	$\varepsilon_{f,e} = 0.17 \left( \frac{f_{cm}^2}{E_f \rho_f} \right)^{0.3} \varepsilon_{fu}$	Fully-wrapped CFRP (or properly anchored CFRP) – FRP fracture controls
	$\varepsilon_{f,e} = \min \left[ 0.65 \left( \frac{f_{cm}^2}{E_f \rho_f} \right)^{0.56} \cdot 10^{-3}; 0.17 \left( \frac{f_{cm}^2}{E_f \rho_f} \right)^{0.3} \cdot \varepsilon_{fu} \right]$	Side or U-shaped CFRP jackets
FRP reinforcement ratio, $\rho_f$	$\rho_f = 2t_f \sin \alpha / b_w$	For discrete FRP reinforcement
	$\rho_f = (2t_f / b_w)(w_f / s_f)$	For continuous FRP reinforcement

Fib Bulletin 90 (Fib, 2019)

FRP contribution to shear strength	$V_{Rd,f} = \frac{A_{fw}}{s_f} h_f f_{fwd} (\cot \theta + \cot \alpha) \sin \alpha$	
FRP reinforcement ratio, $A_{fw}/s_f$	$A_{fw}/s_f = 2t_f w_f / s_f$	For discrete FRP reinforcement
$s_f$	$A_{fw}/s_f = 2t_f \sin \alpha$	For continuous FRP reinforcement
FRP effective strength, $f_{fwd}$	$f_{fwd} = f_{fwd,c} = k_R \alpha_c f_{fd}$ With, $\alpha_c = 0.8$ and, $k_R = \begin{cases} \frac{0.5r_c}{50} \left(2 - \frac{r_c}{50}\right), & r_c < 50 \text{ mm} \\ 0.5, & r_c \geq 50 \text{ mm} \end{cases}$ $f_{fwd} = \text{minimum}\{f_{fbwd}; f_{fwd,c}\}$	For fully-wrapped or properly anchored FRP
	Where, For $\frac{h_f}{\sin \alpha_f} \geq l_e$ and $l_e \leq \frac{s_f}{(\cot \theta + \cot \alpha) \sin \alpha_f} \leq \frac{h_f}{\sin \alpha_f}$ : $f_{fbwd} = f_{bk} / \gamma_{fb}$	
	For $\frac{h_f}{\sin \alpha_f} \geq l_e$ and $\frac{s_f}{(\cot \theta + \cot \alpha) \sin \alpha_f} \leq l_e$ : $f_{fbwd} = \left[1 - \left(1 - \frac{2m \cdot s_f}{3 l_e}\right) \frac{m}{n}\right] \frac{f_{bk}}{\gamma_{fb}}$	For U-shaped FRP
	For $\frac{h_f}{\sin \alpha_f} \leq l_e$ and $\frac{s_f}{(\cot \theta + \cot \alpha) \sin \alpha_f} \leq \frac{h_f}{\sin \alpha_f}$ : $f_{fbwd} = \frac{2 (ns_f) / [(\cot \theta + \cot \alpha) \sin \alpha_f] f_{bk}}{3 l_e \gamma_{fb}}$	
Number of FRP strips crossed by shear crack, $n$	$n = \text{integer}\{h_f (\cot \theta + \cot \alpha) / s_f\}$	
Number of FRP strips for which the bond length is less than $l_e$ , $m$	$m = \text{integer}\{l_e (\cot \alpha_f + \cot \theta) \sin \alpha_f / s_f\}$	
FRP bond strength, $f_{fbk}$	$f_{fbk}(s_r) = \begin{cases} \sqrt{\frac{E_f s_{0k} \tau_{b1k}}{t_f} \frac{s_r}{l_e} \left(2 - \frac{s_r}{l_e}\right)}, & s_r < l_e \\ \sqrt{\frac{E_f s_{0k} \tau_{b1k}}{t_f}}, & s_r \geq l_e \end{cases}$	
Effective bond length, $l_e$	$l_e = l_{b,max} = \frac{\pi}{2} \sqrt{\frac{E_f t_f s_{0k}}{\tau_{b1}}}$ With $s_{0k} = 0.20 \text{ mm}$	
Characteristic value of maximum bond stress, $\tau_{b1k}$	$\tau_{b1k} = \begin{cases} 0.37 \sqrt{f_{cm} f_{ctm}}, & \text{for CFRP strips} \\ 0.44 \sqrt{f_{cm} f_{ctm}}, & \text{for CFRP sheets} \end{cases}$	